Pseudo 2D ecosystem model for a dendritic reservoir

*Alberto de la Fuente**, *Yarko Niño*

Departamento de Ingeniería Civil, Universidad de Chile, Santiago, Chile

A B S T R A C T

A two-step methodology is presented for long-term eco-hydrodynamic simulation of a dendritic reservoir that can be subdivided into many interacting subsystems. This approach provides a balance between spatial resolution and simulation time extent. The first step aims at defining the exchange mass and water fluxes among basins. The second step is the eco-hydrodynamic modelling of the subsystems. This methodology is applied to Rapel reservoir, located in central Chile, which can be subdivided into three distinct basins. For this application, a 2D depth-averaged model is used to define exchange fluxes at the basin confluence, while a 1D, horizontally-averaged, vertically resolving model is used to simulate the hydrodynamics and biochemical behaviour of each basin. Dimensional analysis is introduced to analyse the water quality simulations and to determine whether internal processes or external loading are dominant and better explain the measured differences in phytoplankton biomass among the basins. The product of biomass growth rate and basin retention time is identified as an important dimensionless parameter describing the associated dynamics.

Keywords:
Rapel reservoir
Reservoir hydrodynamics
Water quality
Numerical modelling
Phytoplankton dynamics
DYRESM-CAEDYM
AQUASEA

1. Introduction

Ecosystems are open systems, involving matter/energy/information flows from and to the surrounding environment. They may be described in terms of flows and compartments: i.e., by adopting a network perspective (Bendoricchio and Palmeri, 2005). In the case of aquatic ecosystems, such as those of lakes and reservoirs, this approach can be followed by posing a set of N mass transport equations to model the dynamical behaviour of an equal number of species representing state variables of the system. Typically, source and sink terms are used in those equations, to address internal (chemical/biological) changes within the ecosystem. The hydrodynamics of the water body, and the presence of inflows and outflows, define the nature and direction of fluxes that are to be present in the model.

At present, due to the increase in computational power and advances in the development of numerical techniques, there are several hydrodynamic models available, in 1, 2 or 3 spatial dimensions, to simulate mass transport processes in lakes and reservoirs, which are typically coupled with a biochemical module to account for mass transformations within the ecosystem (e.g., Hamilton and Schladow, 1997; Jørgensen and Bendoricchio, 2001; Staskraba and Hocking, 2002; Gal et al., 2003; Loose et al., 2005). Usually, these models are used to estimate pollutant concentrations, to predict future environmental conditions at sites of interest due to changes in external conditions, to predict future eutrophication conditions, to define maximum nutrient loads to prevent eutrophication, etc. (e.g., Artioli et al., 2005; Porcasi et al., 2005; Knightes and Cyterski, 2005).

In choosing a particular hydrodynamic model there is an obvious conflict between higher spatial dimensionality and restrictions such as availability of data for calibration/validation and the ability to do long-term simulations. Three-dimensional models, offer good spatial resolution of

* *Corresponding author*.
E-mail addresses: aldelafu@ing.uchile.cl (A. de la Fuente), ynino@ing.uchile.cl (Y. Niño).

internal processes, being then useful tools for studying different processes that modulate the ecosystem dynamics (e.g., Botelho and Imberger, 2007), the impact that produces an external agent acting on the ecosystem (e.g. Spillman et al., 2007), or the dynamics of algae bloom events (Robson and Hamilton, 2004). Usually, these high spatial resolution models require also a high temporal resolution of the input forcing data. Likewise, calibration/validation require in-lake measurement of physical and biochemical parameters with high enough spatial resolution as to capture the spatial variability of the system that is expected to be resolved by the numerical simulations.

On the other hand, one-dimensional (horizontally averaged) models, provide only vertical resolution of internal processes, but operate with less input information and require less data resolution for validation and calibration. Furthermore, they can be run for longer time spans, often at a multi-annual level. For instance, applications aimed at characterizing seasonal stratification (Patterson et al., 1984; Gal et al., 2003), the role of zooplankton on the annual cycling of nutrients (Bruce et al., 2006), or to analyse the long-term evolution of pit lakes (Castendyk and Webster-Brown, 2007) have been successfully carried out.

In between these two approaches, models of different dimensionality can be combined in order to find a balance between spatial resolution, long-term modelling, and available data. For instance, Romero et al. (2004) have carried out a 2 years long simulation with a 1D model (DYRESM-CAEDYM, Imberger and Patterson, 1981; Hamilton and Schladow, 1997) in two lakes, in order to identify the dominant processes affecting nitrogen and phosphorus cycling, and have studied in detail by means of a 3D model (ELCOM, Hodges et al., 2000) one flood event in which advection is the predominant process.

There is a clear limitation of 1D models in the case of systems with complex geometry, such as reservoirs with dendritic geometry, particularly where the subsystems or basins of the reservoir exhibit different hydrodynamic and ecosystemic behaviour. In such case the hypothesis of horizontal homogeneity cannot be invoked, and furthermore the hydrodynamic exchange between subsystems must be captured in order to understand the dynamics of the whole system.

The aim of the present paper is to show how low dimensionality models (1D and 2D) can be applied together with available data to learn about the dynamics of a system, particularly a dendritic reservoir. This would be the first step to design appropriate field campaigns to gain the required information to further validate the results of the simulations prior to applying higher dimensionality models to improve the knowledge of the water body and to design management alternatives to restore or improve the quality of the associated environmental system (Imberger, 2005).

Application of the proposed methodology makes sense in developing countries, where the lack of data is a common situation that has to be faced when trying to apply eco-hydrodynamic models to lakes and reservoirs. In Chile, for instance, water agencies maintain a monitoring system that includes only 15 lakes and reservoirs, and in-lake physical and biochemical data is measured at a seasonal level (www.dga.cl). Only a few systems have meteorological and hydrological data available, and water quality data is often lacking or incomplete. Application of high dimensional models in systems with little information is clearly not possible and the analysis of such systems must start by the building of a database and by conducting field campaigns to acquire the necessary data to calibrate/validate the simulations.

2. Application to Rapel reservoir

This paper focuses on Rapel reservoir, a monomictic, temperate fresh water body located near the coast in central Chile (33°S) (Contreras et al., 1994; Vila et al., 1997). The reservoir supplies Rapel hydropower plant and receives the treated effluents of a mining tailings reservoir located nearby. The main inflows to the reservoir are Cachapoal and Tinguiririca rivers, which drain an extensive catchment with mining and agricultural activities. By the end of the 1980s massive fish kills occurred in the reservoir, specifically at the confluence of Alhué and Cachapoal basins (Fig. 1). Furthermore, evidence indicates that water quality in the reservoir has been declining in time due to anthropogenic effects (Vila et al., 1997; Ahumada, 2000).

A limited database is available for this system. In-lake temperature and water quality data were collected between January 1991 and March 1992, at a monthly interval at several stations within the reservoir by limnologists of the Department of Ecology, Universidad de Chile (Martinez et al., 2003). In addition, meteorological and hydrological forcing data, taken at a daily level by ENDESA (the company that operates Rapel hydropower plant) and DGA (Chilean Water Agency), are available for the same period. Unfortunately, no corresponding inflow water quality data is available.

Rapel reservoir has a dendritic morphology (Fig. 1), with three main basins. As the application of a 3D model to this system is not possible due to the lack of the necessary data, and 2D depth-averaged models do not capture the vertical structure of the water column, which is known to become stratified in the summer season at least in part of the reservoir (Vila et al., 1997), an alternative strategy is proposed in this paper. It involves applying a 1D horizontally averaged (i.e., vertical resolving) model to each basin separately, for which the mass exchange between basins has to be previously determined. To accomplish this, a 2D depth-averaged model is applied to the confluence of the basins. The 1D model used in the simulations (DYRESM-CAEDYM, Imberger and Patterson, 1981; Hamilton and Schladow, 1997) allows for multi annual modelling, however the 2D model used (AQUASEA, Kjaran et al., 2004) can be applied for only a few days without losing accuracy. To overcome this problem, the analysis of the mass exchange at the confluence of the basins was done for different hydrodynamic conditions in the reservoir, including those associated with mean values of the inflows as well as floods.

To overcome the lack of inflow water quality data, the eco-hydrodynamic model used is considered as a black box, such that an input can be correlated with its corresponding output. Consequently, inflow water quality data is calibrated in order to obtain in-lake water quality parameters in agreement with available field measurements. In the process, the models provide insight regarding the main phenomena controlling the behaviour of the reservoir.

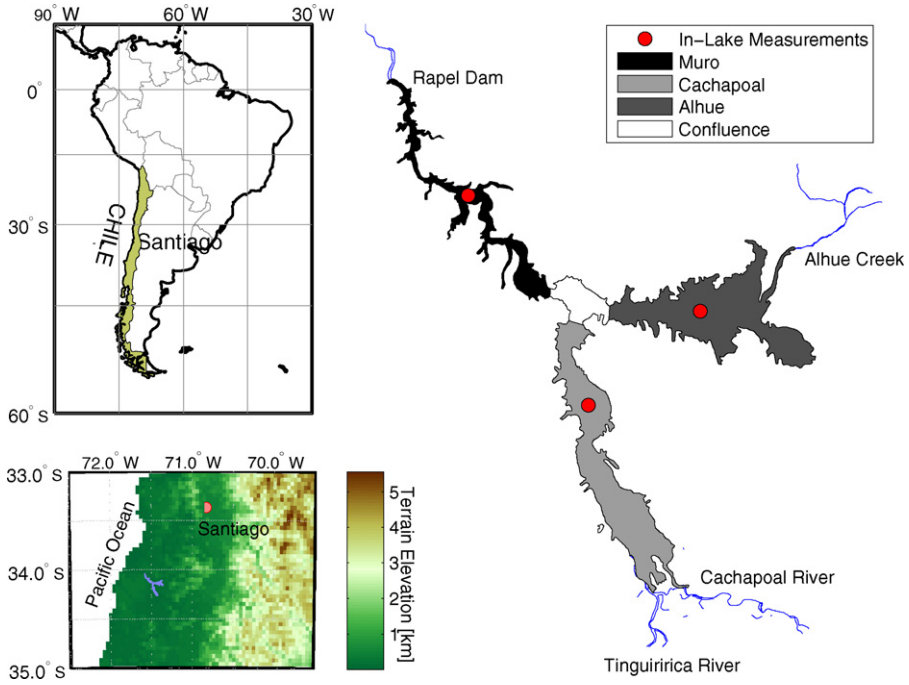

Fig. 1 – Location of Rapel reservoir in Chile and basin subdivision.

3. Reservoir characteristics and data available

Rapel reservoir was formed by the construction, in 1968, of an arch dam that closed Rapel river for hydropower generation. The dam is 85 m tall, the area flooded is about 80 km^2, and the total volume of the reservoir is about 700 Hm^3. The hydropower plant can produce 350 MW of electricity through the operation of 5 engines, with maximum flow capacity of 105 $m^3\,s^{-1}$ each.

The hydrological regime of inflows to the reservoir is mainly pluvial, with maximum discharges occurring during winter. Main inflows to the reservoir are Cachapoal and Tinguiririca rivers, with 180 and 100 $m^3\,s^{-1}$ of daily average flow in winter, and 100 and 40 $m^3\,s^{-1}$ in summer, respectively. The highest flows are about 2000 $m^3\,s^{-1}$ for each river during winter rainfall. A third, less important inflow is Alhué creek, with a monthly average flow of about 20 $m^3\,s^{-1}$. Winter floods in this stream reach values of about 200 $m^3\,s^{-1}$.

The three basins of the reservoir can be described as follows: (i) Alhué (north-eastern basin) is characterized by the shallowest waters (about 17 m deep), smallest volume (120 Hm^3), and lowest inflows (Alhué creek), which produce the largest retention time (about 73 days); (ii) Cachapoal (south-eastern basin) receives waters from Cachapoal and Tinguiririca rivers, has a maximum depth of 24 m, a volume of 210 Hm^3, and a mean retention time of about 8.7 days; (iii) Muro (north-western basin), limited by Rapel dam and affected by the operation of the hydropower plant, has a volume of 340 Hm^3, a maximum depth of 85 m, and a mean retention time of about 13.2 days. There are two outlets for outflows, one, placed at 35 m above the bottom, for hydropower generation, and the other, corresponding to two controlled spillways, located 70 m above the bottom.

The meteorological forcing data used for modelling show mean daily values of air temperature of 15 °C with maximum and minimum daily values of 24 and 4 °C, respectively. Daily solar radiation oscillates between 25 and 325 W m^{-2}, and wind speed shows maximum daily values of 6.3 ms^{-1} for the time period analysed in this study. Fig. 2 shows mean daily values of inflows and outflows for that period. In-lake measurements of nutrients and chlorophyll concentration were taken at locations shown in Fig. 1, at three different depths, 0, 5 and 10 m in Cachapoal and Alhué basins, and 0, 17 and 35 m in Muro basin. Fig. 3 shows the mean water column NH_4

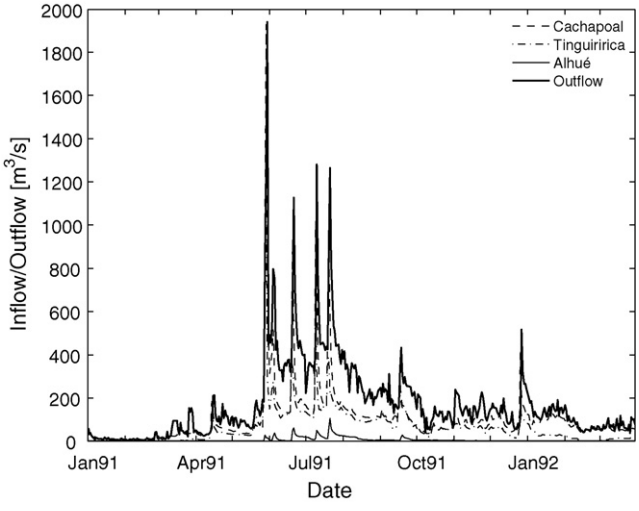

Fig. 2 – Inflow and outflow data for the period of analysis.

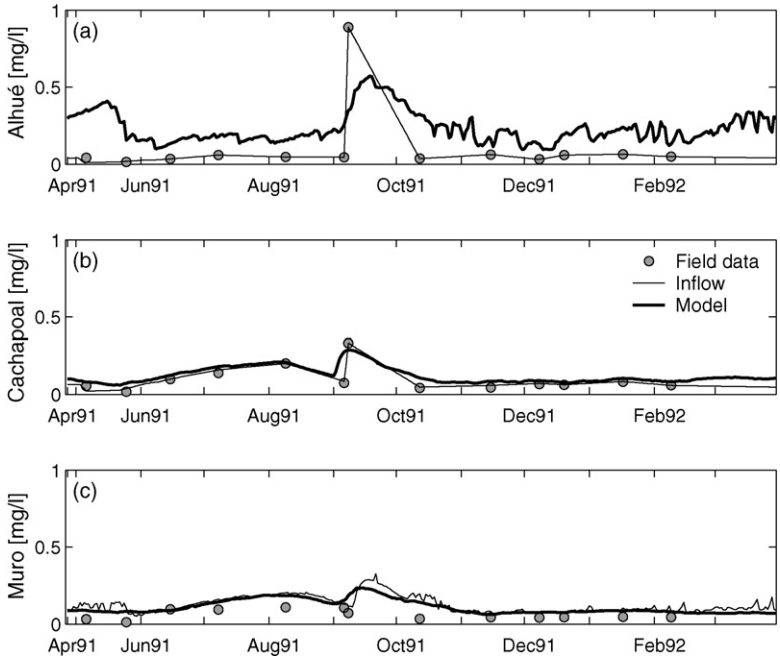

Fig. 3 – Simulated (dark line), observed (grey dots) and assumed inflow concentration (light line) of NH_4 [mg l^{-1}] for Alhué, Cachapoal and Muro basin (panels a, b and c, respectively).

concentrations in each basin during the period of observation (January 1991–March 1992), and Figs. 4 and 5 plot the same concentration for PO_4 and NO_3, respectively. Nutrient concentrations appear to be highest in Cachapoal basin and lowest in Alhué basin, where some very small values of phosphorus concentration (under detection limits equal to 0.003 mg l^{-1}) were observed (Figs. 3–5). Furthermore, measurements of phytoplankton biomass, based on chlorophyll a concentration (*Chla*), show that maximum values occur generally during the spring–summer period, except in Alhué basin, where this biomass is rather constant throughout the year and always higher than in the rest of the reservoir, particularly during winter (Fig. 6). The trophic state of these basins, based on TSI index (Carlson, 1977), corresponds to mesotrophic in Cachapoal and Muro basins (TSI = 53 and 54, respectively), and eutrophic in Alhué basin (TSI = 63).

Vertical profiles of temperature, dissolved oxygen, conductivity and salinity, measured during the summer of 1995 in

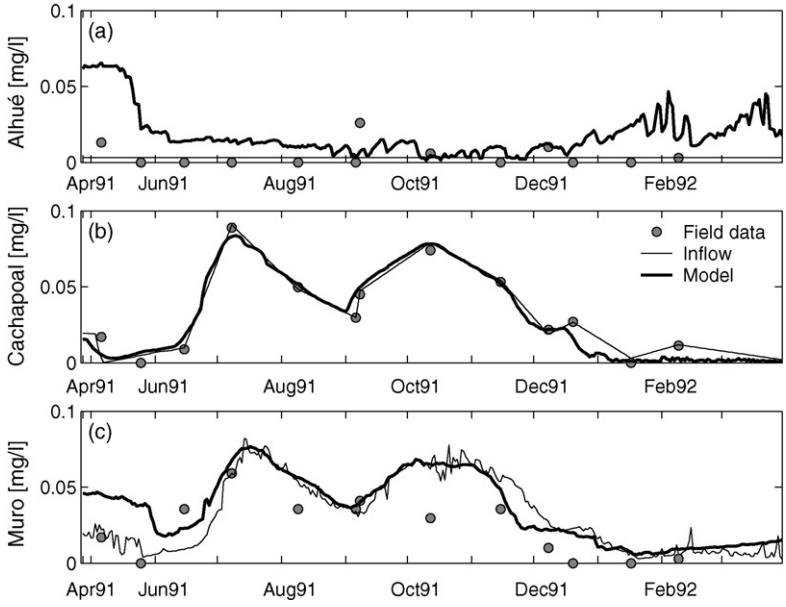

Fig. 4 – Simulated (dark line), observed (grey dots) and assumed inflow concentration (light line) of PO_4 [mg l^{-1}] for Alhué, Cachapoal and Muro basin (panels a, b and c, respectively).

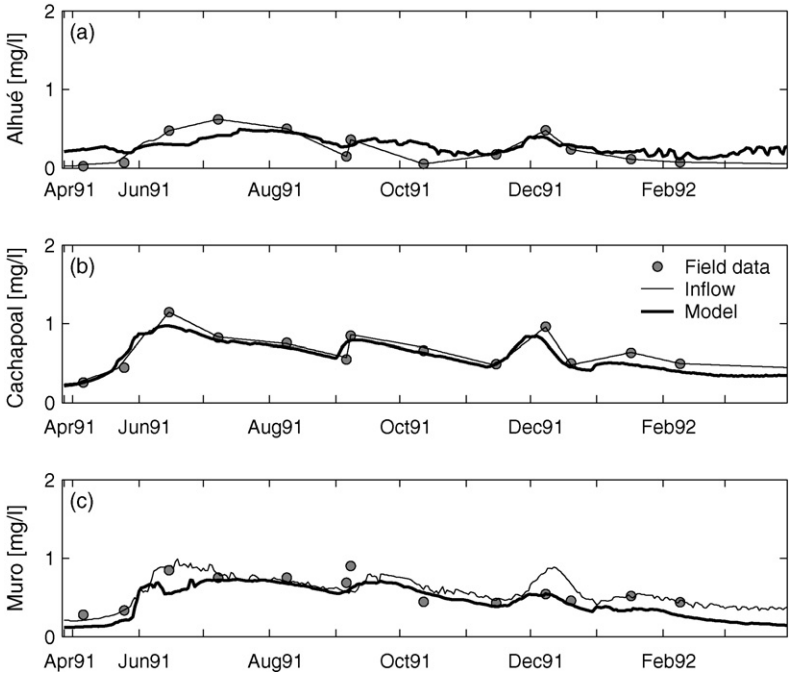

Fig. 5 – Simulated (dark line), observed (grey dots) and assumed inflow concentration (light line) of NO_3 [mg l^{-1}] for Alhué, Cachapoal and Muro basin (panels a, b and c, respectively).

Muro basin (Vila et al., 1997) are shown in Fig. 7. No similar profiles are available for the observation period of 1991–1992. In that period, only local values of the water properties presented in Fig. 7 were measured at different stations and depths within the reservoir. Based on the information available, it is reasonable to assume that the profiles measured in Muro basin in the summer of 1995 are fairly representative of predominant conditions occurring during summer in that basin, particularly during the period of analysis of 1991–1992. The vertical profiles shown in Fig. 7 indicate the presence of a thermocline located at about 35 m above the reservoir bottom, an extremely high salinity gradient at the same level, and anoxic conditions in the hypolimnion.

4. Hydrodynamics and water quality modelling

Time evolution of vertical heat and mass transport and water quality within each basin of the reservoir was modelled using DYRESM-CAEDYM. Vertical density structure within the reservoir was obtained from its temperature and salinity structure

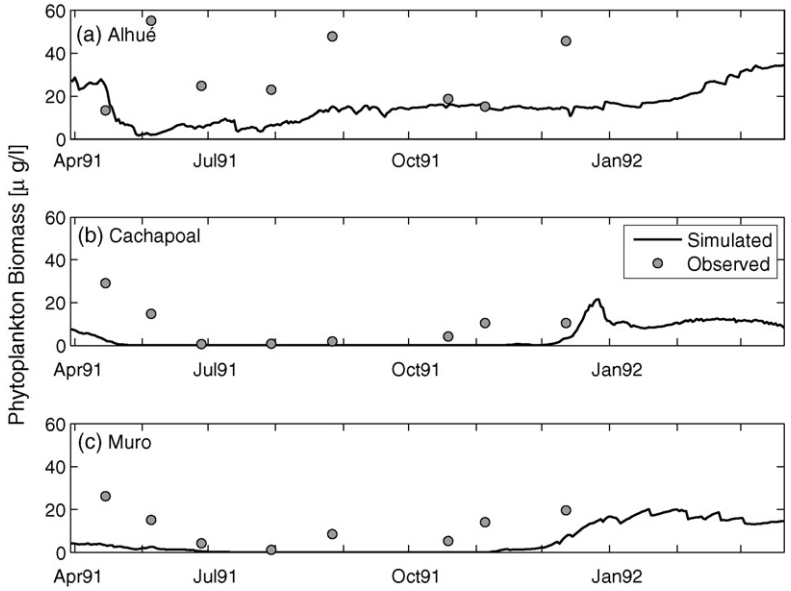

Fig. 6 – Simulated and measured values of chlorophyll a concentration (*Chla*) in each basin.

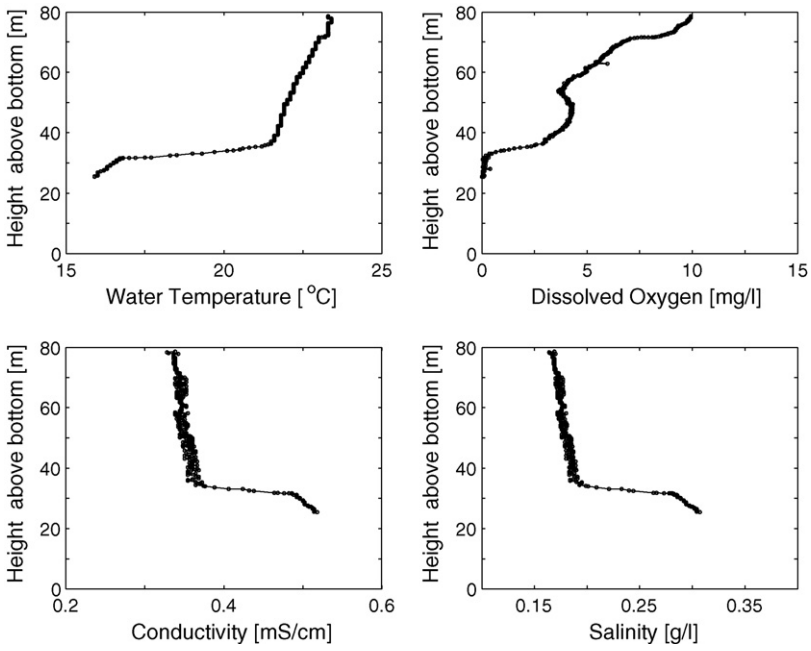

Fig. 7 – Vertical profiles of temperature, dissolved oxygen, conductivity and salinity, measured in the summer of 1995 in Muro basin.

computed with DYRESM forced at a daily level with the available meteorological and hydrological data.

1D simulations with DYRESM-CAEDYM have been done successfully in many lakes and reservoirs around the world (Antenucci, 1996; Han et al., 2000; Romero et al., 2004; Bruce et al., 2006). However, 2D or 3D phenomena in lakes dynamics, such as upwelling or circulations induced by Coriolis effect, should not be important in order to apply the model (see CWR, 2004 and Fischer et al., 1979). These limitations were verified by Antenucci (1996) and in the present application: the seasonal thermocline in Muro basin is too deep for upwelling to occur and, on the other hand, the reservoir is narrow enough as to safely neglect Coriolis effects.

Two phytoplankton groups (fresh water diatoms and chlorophytes) were selected as state variables of the system, as they are the dominant phytoplanktonic groups present in this reservoir (Vila et al., 1997 and Martinez et al., 2003). Their dynamics was simulated as function of the water temperature (T), nutrient concentrations (NO_3, PO_4 and NH_4), and light intensity (I). In this analysis, grazing by zooplankton is neglected, as are salinity effects on phytoplankton mortality rate because of the low values of this variable measured in the reservoir (much less than $1\,mg\,l^{-1}$). Also, given the high values of silica concentration measured in the reservoir (of about $2\,mg\,l^{-1}$) it is assumed that diatoms are not limited by this element. No other biological compounds, such as bacteria or zooplankton, were included in the analysis, mainly because there are no data available to do the respective validation of the simulations results. Besides, previous studies do not identify them as central elements to be considered in the analysis of the reservoir ecology (Vila et al., 1997; Martinez et al., 2003).

Water quality simulations were done based on the standard functions used in CAEDYM to represent the rate of change of the algae biomass (Hamilton and Schladow, 1997; CWR, 2004; Robson and Hamilton, 2004; Romero et al., 2004; or recently, Spillman et al., 2007), where the time evolution of the biomass of each phytoplankton group, measured in terms of *Chla*, is determined from a first order reaction of the type:

$$\frac{\partial Chla_j}{\partial t} = \Psi\, Chla_j \tag{1}$$

where $Chla_j$ denotes biomass of phytoplankton group j, and Ψ is the net growth rate specific for this phytoplankton group, which is function of the nutrient availability, water temperature and light intensity. Biomass losses due to sedimentation are also represented by a first order reaction type equation similar to Eq. (1).

Values of parameters that describe the phytoplankton dynamics are shown in Table 1. Those values, as well as other constants used for the simulations, were defined based on template files of CAEDYM V 1.4 (CWR, 2004). Due to the lack of sufficient data, the focus of the present analysis was on identifying the main agents controlling the phytoplankton dynamics in the different basins of the reservoir rather than on a precise determination of the state variables and water quality model constants.

The flow and mass exchange at the confluence of the basins was analysed using a 2D, depth-averaged model. According to field observations, the water column is not stratified in this region. AQUASEA is a commercial software that solves the standard 2D Saint-Venant equations using a finite element scheme (Kjaran et al., 2004). Further detail about the numerical scheme can be found in Kjaran et al. (2004) or in the web page www.vatnaskil.is/aquasea.htm.

A mesh of 2403 triangular elements was created to cover the entire area of the reservoir (about $80\,km^2$). The model was forced with surface level, inflow and outflow data corre-

Table 1 – Constants used to model phytoplankton dynamics

	Symbol	Unit	Chlorophytes	Diatoms
Growth rate	μ_{max}	day^{-1}	1.750	1.950
Respiration rate	μ_r	day^{-1}	0.200	0.140
Temperature multiplier for respiration	θ_r	–	1.070	1.080
Temperature multiplier for growth	θ_g	–	1.070	1.060
Standard temperature		°C	20	14
Optimum temperature		°C	29	15
Maximum temperature		°C	38	29
Photosynthesis-irradiance curve parameter		$\mu E\,m^{-2}\,s^{-1}$	60	30
Half saturation constant for phosphorus		$mg\,l^{-1}$	0.002	0.002
Half saturation constant for nitrogen		$mg\,l^{-1}$	0.02	0.0023
Settling velocity		ms^{-1}	1.74×10^{-6}	9.3×10^{-6}

Table 2 – Flow rate data for AQUASEA hydrodynamic simulations in $m^3\,s^{-1}$

	Day	Cachapoal	Tinguiririca	Alhué Creek	Outflow
Run 1	September	121.3	110.7	7.7	216.51
Run 2	26/05/91	60.7	104.0	0.8	208.5
	27/05/91	248.0	196.0	1.7	352.4
	28/05/91	984.0	690.0	29.3	403.4
	29/05/91	1928.0	1098.0	32.1	851.0
	30/05/91	883.0	304.0	9.8	664.8
	31/05/91	456.0	205.0	4.7	362.8

Run 1 considers the monthly average of the flow rate for September 1991, and Run 2 the 6 days flood of 1991.

sponding to two different flow situations, both representing increasing volume conditions within the reservoir. Those situations correspond to: Run (1) constant inflows and outflows equivalent to monthly average values for the month of September, which can be considered as representative of mean hydrologic conditions in the reservoir, and Run (2) the "great flood" of 26–31 of May, 1991. Table 2 shows discharge data for both conditions.

To analyse mass exchange at the confluence of the basins, the mass transport equation was solved for the two scenarios described in Table 2. For this analysis, an initial condition consisting of a null concentration of a non-reactive tracer was imposed in the entire reservoir, except in the 2.5 km^2 area corresponding to the confluence zone, where the concentration was initialised with an arbitrary value equal to unity.

5. Method of analysis

5.1. *Rate of change analysis*

By doing a simple mass balance analysis within a control volume for a general variable, Φ, assuming conservation of volume accounting for inflows and outflows, that mass is homogeneously distributed in space, and considering the rate of change of Φ given by an expression such as Eq. (1), the following dimensionless governing equation is obtained:

$$\frac{\partial \Phi^*}{\partial t^*} = (\Pi_1 - 1)\,\Phi^* + \Phi^*_{in} \tag{2}$$

where $\Pi_1 = \Psi\Theta$, Θ, is the retention time, defined as the ratio between the water volume and water inflow discharge, Ψ denotes, once again, the rate of change of Φ caused by internal processes, $\Phi^* = \Phi/\Phi_{ref}$ and $\Phi^*_{in} = \Phi_{in}/\Phi_{ref}$, where Φ_{in} is the inflow concentration of Φ and Φ_{ref} a reference concentration of Φ. $t^* = t/\Theta$ is the dimensionless time. Eq. (2) shows that the temporal changes of Φ are controlled by internal processes, but also by the inflow concentration. The dimensionless parameter $\Pi_1 = \Psi\Theta$ can be used to assess whether in-lake concentrations are determined mainly by internal processes or by inflow concentration. Indeed, Π_1 indicates how fast are the internal changes compared with the natural timescale of the lake, Θ. Therefore, a value $\Pi_1 > 1$, that is a large Θ with respect to Ψ, implies that time variation of Φ depends mainly on internal changes rather than on external inputs. On the other hand, $\Pi_1 < 1$, that is for small retention times or slower internal processes, values of Φ are always close to Φ_{in}.

A similar analysis can be conducted by considering those processes that involve interfacial mass transport through the lake surface or the bottom sediments. Those processes are characterized by a dimensionless parameter,

$$\Pi_2 = \frac{v_s\,\Theta}{H_e}, \tag{3}$$

which is defined as the ratio between the timescale of the lake, Θ, and the timescale that indicates how fast the interfacial transfer is, H_e/v_s, where v_s denotes the transport velocity, such as the settling velocity or gas exchange coefficient, and H_e is the mean depth of the lake or basin.

Considering mass exchange processes requires a slight modification of Eq. (2), however such exchange can also be expressed as a first order reaction (e.g. Jähne and Haußecker, 1998). A parameter such as Π_2 can provide the neces-

sary scaling in order to compare the relative importance of these processes with internal processes or external loading accounted for by the parameter Π_1.

5.2. *Error analysis*

Two indicators are used to interpret the numerical results and both are defined based on a rate of change analysis rather than on the direct comparison of observed and simulated concentrations. The first indicator, denoted $\Delta\theta$, is used to assess the importance of internal processes versus external inputs on the determination of in-lake concentrations. Particularly, it is used to quantify how good the assumed inflow nutrient concentrations are. $\Delta\theta$ is defined as:

$$\Delta\theta = 100\frac{1}{N_T}\sum_{tn=1}^{N_T}\frac{\theta_{tn}-\theta_{in}}{\bar{\theta}_{in}} \tag{4}$$

where θ_{tn} denotes the simulated in-lake concentration at time $tn = n\,\Delta t$, Δt is the time interval used in the simulation, θ_{in} denotes the estimated inflow concentration for the same time, N_T is the total number of time steps of the simulation, and $\bar{\theta}_{in}$ is the mean estimated inflow concentration of θ.

If the in-lake concentration θ is lower than the inflow concentration θ_{in}, then $\Delta\theta$ is negative and internal processes consume mass. On the other hand, if $\Delta\theta > 0$, then internal processes increase θ and $\Delta\theta$ indicates the produced fraction of this variable with respect to θ_{in}. Also, $\text{abs}(\Delta\theta) \approx 0$, indicate that in-lake concentrations are basically equal to corresponding inflow inputs θ_{in}, and thus the system state is dictated primarily by those inputs. In such a case an acceptable calibration for the inflow concentrations is to consider them equal to the observed in-lake data. On the other hand, high values of $\text{abs}(\Delta\theta)$ indicate that the system state is mainly governed by internal processes and thus the inflow concentrations are nearly irrelevant in determining that state. In such a case, precise calibration of inflow concentrations is not possible and rather unnecessary.

The second indicator, denoted ε_Φ, is used to quantify the phytoplankton simulation error, but expressed in terms of the rate of change of phytoplankton biomass rather than in terms of the biomass itself. The definition of ε_Φ is based on the fact that, in general, the rate of change of any variable Φ is expressed as a first order reaction (Eq. (1)), such that the error in such rate of change can be expressed as:

$$\varepsilon_\Phi = \frac{100}{N_f}\sum_{tf=1}^{N_f}\frac{|\Psi_s^{tf}-\Psi_o^{tf}|}{\bar{\Psi}_o} \tag{5}$$

where the subindexes s and o denote values of Ψ calculated using simulated and observed in-lake data, respectively, N_f is the number of the available field data points and $\bar{\Psi}_o$ is the mean value of Ψ_o, using the N_f in-lake measurements. This indicator gives an estimate of the absolute value of differences between observed and predicted rates of change of primary variables

6. Results and discussion

6.1. *Hydrodynamic interaction among the basins*

2D simulations of the hydrodynamic interaction between basins were conducted for cases when the water volume in the reservoir increases. These were aimed mainly at describing the process of water injection from Cachapoal basin into Alhué basin. Simulation results of Run 1 (Table 2), shows that water from Cachapoal basin does not enter to Alhué basin, even though the mass balance within the reservoir indicates that the water volume was increasing (Fig. 8). Furthermore, the simulation yields a negligible velocity in Alhué basin, which is clear evidence that this basin is isolated from the rest of the reservoir under normal hydrologic conditions. On the other hand, simulation of the great flood of 1991 shows that water from Cachapoal basin does enter Alhué basin (Fig. 9). Despite this, the computations show that the volume of water that enters Alhué basin is just that which is needed to compensate the increase in water table levels within the reservoir, and that during the receding part of the hydrograph this volume exits this basin back toward Muro basin. It is found that during flood conditions the water that enters to Alhué basin is not entirely mixed within the basin, thus showing that even under extreme hydrological conditions the exchange of water between Alhué basin and the rest of the reservoir is rather weak.

Simulation of mass transport at the basin confluence zone confirms the previous conclusion. The numerical results show that mass placed within the confluence zone at the beginning of the flood does not completely enter Alhué basin at the period of highest advective transport from Cachapoal to Alhué basins, and that by the end of the flood the mass is transported back towards Muro basin (see Fig. 10).

From these results it is concluded that mass present in Cachapoal basin is not a relevant mass source for Alhué basin, not even during major flood events.

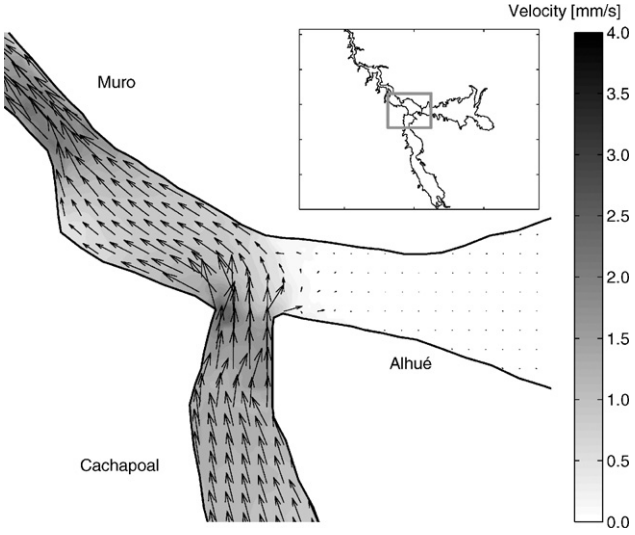

Fig. 8 – Simulated flow velocity field in the basins confluence zone for September mean conditions. Right-upper plot shows the zoomed confluence area within Rapel reservoir.

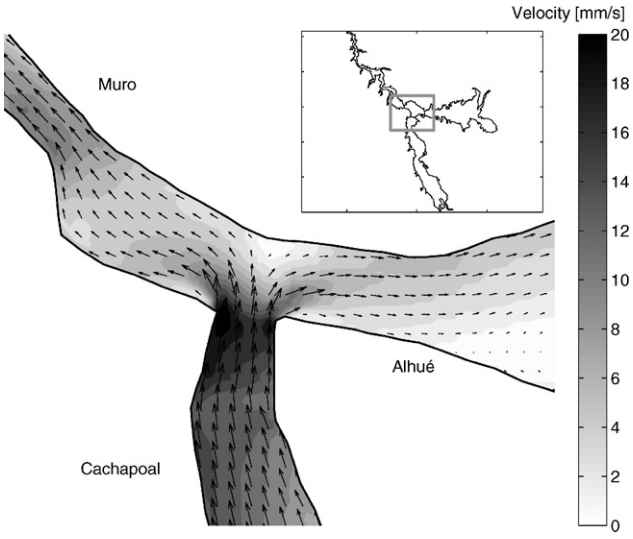

Fig. 9 – Simulated flow velocity field in the basins confluence zone at 1991 flood peak. Right-upper plot shows the zoomed confluence area within Rapel reservoir.

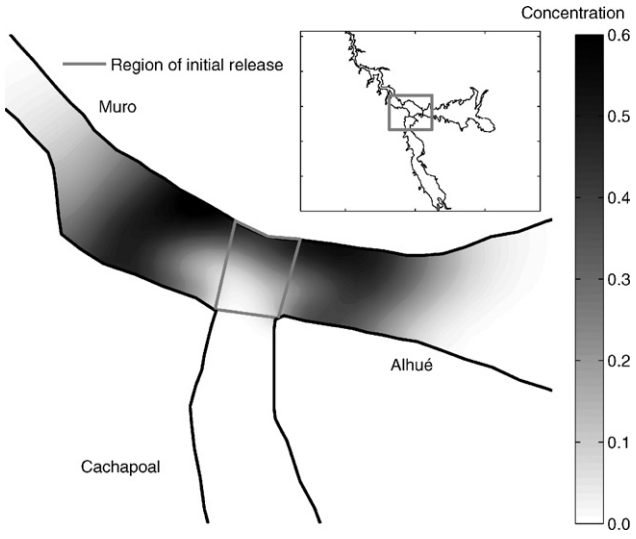

Fig. 10 – Concentration distribution, at the end of a 6 days computation, of a conservative species which was placed uniformly distributed within the basins confluence zone, at the beginning of the 1991 flood. Right-upper plot shows the zoomed confluence area within Rapel reservoir.

This result provides a criterion to establish a conceptual model for interactions among the basins, which can be summarized as follows: under normal hydrologic conditions, water from Cachapoal and Alhué basins flows into Muro basin, being the contribution of the latter less than 5% of the former; during floods, water from Cachapoal basin flows mainly into Muro basin and also, to a lesser extent, into Alhué basin, to compensate the volume required to equalize the water surface elevation in the reservoir, nonetheless that same water exits towards Muro basin at the end of the flood, providing a negligible net input of dissolved or suspended species from Cachapoal to Alhué basins.

This conceptualization of the hydrodynamic interaction among basins was used to define inflow and outflow conditions required to apply DYRESM and CAEDYM models to each individual basin.

6.2. *Vertical mixing*

Fig. 11 presents a comparison between simulated and measured surface water temperatures during the period of analysis for each basin. It shows that the present simulations reproduce fairly well the observed time variation of surface temperatures within the reservoir.

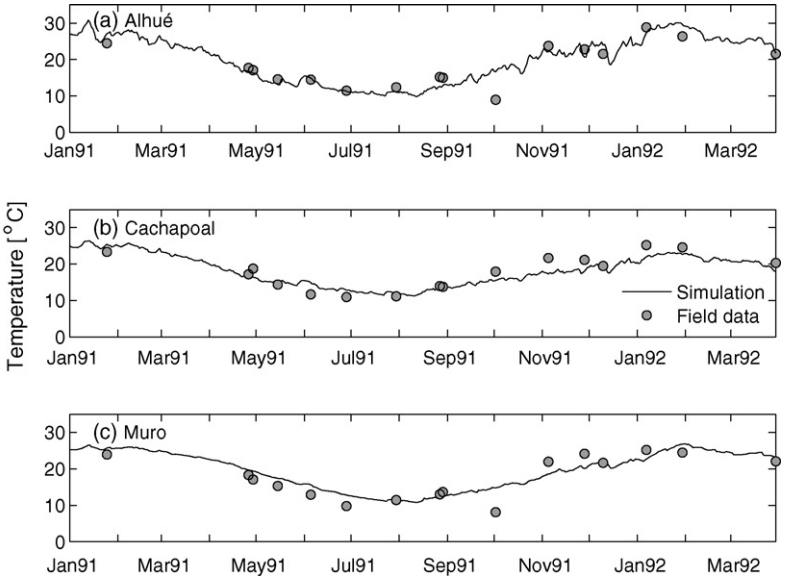

Fig. 11 – Simulated and observed surface water temperatures in each basin (°C).

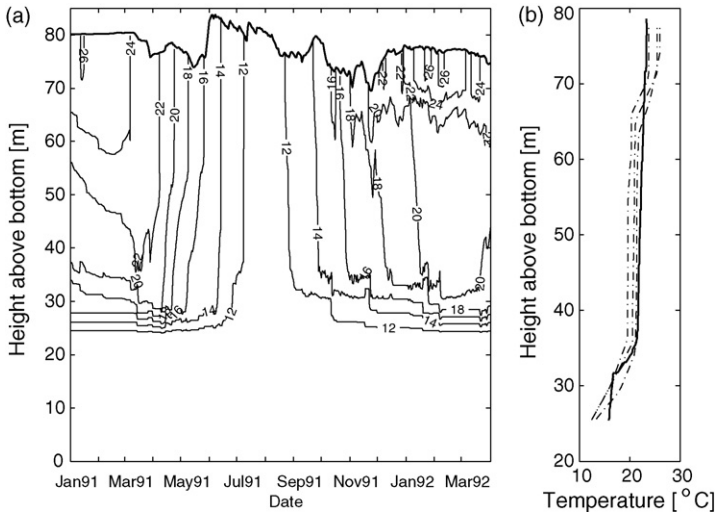

Fig. 12 – Simulated time evolution of vertical temperature profile in Muro basin (panel a), and comparison of simulated profiles for January 1, 15 and 30, 1992 (dashed lines) and measurements (solid line) shown in Fig. 7 (panel b).

A similar result was obtained for water temperatures at other depths. These results show that during the cooling season water temperatures in each basin are similar, but during the summer, water temperature in Alhué basin is a few degrees higher than in the other basins. Coldest waters in the summer are those of Cachapoal basin. This result is clearly related with retention time differences among basins.

Fig. 12a shows the simulated time evolution of the vertical temperature profile in Muro basin, which reproduces fairly well the summer stratification observed in the measured temperature profile shown in Fig. 7 (Fig. 12b). The Numerical simulation locates the seasonal thermocline at 35 m above the reservoir bottom, which is only slightly higher than the observed location of this interface in Fig. 7. Considering, as a reference, the base value of 0.25 m^{-1} for the light extinction coefficient used in the simulations, without accounting for the algae or turbidity effects computed by CAEDYM, it can be predicted that solar penetrative radiation is reduced to less than 1% at a depth of 20 m. Hence, for the thermocline to be located much deeper than this 20 m depth, an important source of turbulent kinetic energy should be available, capable of inducing the diffusion of heat to deeper regions of the reservoir. This source of turbulent kinetic energy is clearly the outlet for hydropower generation, located precisely at 35 m from the reservoir bottom in Muro basin. Simulations of the thermal structure of the reservoir without outflows or inflows showed that the thermocline would be located no deeper than about 20 m from the free surface. These results clearly demonstrate that the operation of Rapel hydropower plant dominates the thermal structure and vertical transport in Muro basin.

6.3. *Water quality simulation*

6.3.1. *Relative importance of internal processes*

Simulations with DYRESM-CAEDYM were carried out for each basin, considering inter-basin exchange fluxes obtained from the hydrodynamic analysis of the confluence zone. Inflow concentration data for Alhué and Cachapoal basins were estimated assuming they correspond directly to the in-lake concentrations (i.e., assuming a priori $\Delta\theta = 0$), considering linear interpolation of in-lake measurements of those concentrations to estimate corresponding time series with a daily frequency. An exception to this criterion corresponds to PO_4 concentration in Alhué creek. Because in-lake measurements were less than the detection limits (10 $\mu g\, l^{-1}$), a constant inflow concentration of PO_4, equal to this limit, was considered as input for this basin. On the other hand, outflows from Cachapoal and Alhué basins are inflows for Muro basin.

The assumptions regarding inflow concentrations to Cachapoal and Alhué basins are considered to be both simple and effective to identify the processes that govern the long-term dynamics of this multibasin reservoir, as shown by the results discussed below.

Figs. 3–5 compare time series of estimated inflow data, depth-averaged in-lake measurements and simulations results for NH_4, NO_3 and PO_4. The indicator $\Delta\theta$ was calculated for each of these nutrients: The results are shown in Table 3. Small absolute values of $\Delta\theta$ indicate that internal processes in Cachapoal basin are negligible compared with the influence of inflows. This means that further study of

Table 3 – Computed values for indicators $\Delta\theta$ and ε_Φ

	$\Delta\theta$		
	NO_3	NH_4	PO_4
Alhué	18.5	163.8	80.7
Cachapoal	−9.7	27.8	−4.9
Muro	−21.9	−12.7	13.0

	ε_Φ	
	Chlorophytes	Diatoms
Alhué	30.3	47.7
Cachapoal	24.4	13.8
Muro	22.5	32.7

this basin should focus on its inflows dynamics rather than on its internal dynamics (see Figs. 3b, 4b and 5b). Something similar occurs with Muro basin (Figs. 3c, 4c and 5c), which also appears to be controlled mainly by the inflows (i.e., the outflows from the other two basins). On the other hand, the highest $\Delta\theta$ values occur in Alhué basin (Figs. 3a, 4a and 5a), indicating that here internal processes control the nutrients dynamics and raise their concentration to about twice that they have in the inflow ($\Delta\theta > 100$). This behaviour indicates that further study of this basin should focus mainly on its internal biochemical processes rather than on its inflow dynamics. Moreover, as the present simulations were not able to adequately reproduce observed concentrations of nutrients, further study should include a broader analysis of the ecosystem in this basin, possibly taking into account more processes and ecological compounds, such as, for instance, particle precipitation, chemical absorption, sediment–water exchange dynamics.

6.3.2. *Phytoplankton simulation*

A reasonable representation of phytoplankton growth rate in each basin is achieved by the model (see Table 3). Estimated values of the mean absolute error ε_Φ for both phytoplankton groups considered are generally lower than 30%. These relatively low ε_Φ values mean that the proposed approach to modelling a multibasin, dendritic reservoir, such as Rapel reservoir, can indeed capture the main processes that govern the phytoplankton dynamics in the system and therefore produce a realistic idea of the general behaviour of the reservoir and main differences between the basins.

This general behaviour is (Fig. 6): Muro and Cachapoal basins present a seasonal variation of *Chla* concentration, with higher values during summer (about 15 $\mu g\,l^{-1}$), and negligible concentrations in winter; Alhué basin presents higher *Chla* concentrations than Cachapoal and Muro basins, and these concentrations are relative high all around the year, with a mean value of about 30 $\mu g\,l^{-1}$.

6.3.3. *Retention time*

First, it is concluded that phytoplankton sedimentation is not relevant in the analysis according with the values of the dimensionless parameter Π_2 given by Eq. (3). This parameter was computed using characteristic values for each basin, and the settling velocity of Table 2. The resulting Π_2 values were much less than 1, with a maximum of 3.9×10^{-3} for Cachapoal basin and freshwater diatoms ($H_e = 24$ m, $\Theta = 8.7$ days and $v_s = 0.8$ m day^{-1}).

Therefore, the different behaviour detected among the basins in terms of both nutrients and *Chla* dynamics are clearly related with retention time, which is much greater in Alhué than in Cachapoal and Muro basins. To clarify this conclusion, values of phytoplankton growth rate Ψ calculated from the simulations are compared with the inverse of the retention time of Eq (2) in Figs. 13a–c. Besides, values of the dimensionless parameter $\Pi_1 = \Psi\Theta$ are plotted in Fig. 13d. Because the phytoplankton inflow concentration was set as 0 for the simulations, the net phytoplankton growth rate is described by $\Psi - \Theta^{-1}$ or $\Pi_1 - 1$ whether Eq. (2) is written in dimensional or dimensionless form, respectively, so from Fig. 13 it is possible to explain the seasonal dynamics of diatoms and chlorophytes, and the functional differences among the basins:

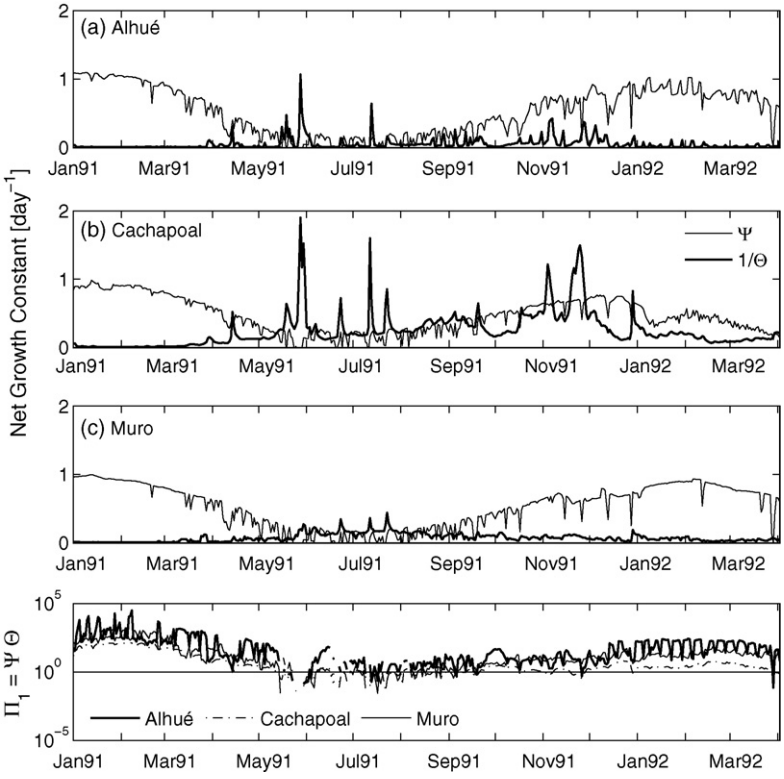

Fig. 13 – Values of Ψ, Θ^{-1}, and Π_1 in each basin during the period of analysis. ($\Psi - \Theta^{-1}$) represents the (dimensional) net phytoplankton growth rate and and ($\Pi_1 - 1$) its dimensionless equivalent.

- Phytoplankton concentrations decrease during winter, despite positive values of Ψ, because of increased flow rates during this season, which rise the retention time value and essentially dilute the biomass in the reservoir. Hence, during winter external influences dominate over internal processes.
- Phytoplankton concentrations increase during summer, mainly because of increased solar radiation and water temperature. This increase is not caused by changes in nutrients availability because their concentrations are, in general, greater than limiting values.
- Simulated and measured values of *Chla* in Alhué basin that are greater than those of the other basins, are explained by a greater retention time of this sub ecosystem, causing net growth rate values that are greater than zero many days during winter, keeping the biomass in this basin relatively high all around the year.

This direct relation between *Chla* concentration and the retention time also applies to nutrient concentrations, which explains differences in the nutrients dynamics among the basins.

7. Conclusions

A two-step methodology has been presented for long time eco-hydrodynamic simulation of a dendritic reservoir that can be subdivided into many interacting subsystems. This approach provides a balance between spatial resolution, to study spatial differences among the subsystems, and simulation time extent. The first step aims at defining the exchange mass and water fluxes among the basins, from the knowledge of their hydrodynamic interactions. The main result of this step is a set of rules that define the mass and water in- and out-fluxes for each one of the basins. The second step corresponds to the eco-hydrodynamic modelling of subsystems, taking into account in- and out-fluxes as well as internal processes.

This methodology was tested in Rapel reservoir, to simulate the associated phytoplankton dynamics (chlorophytes and freshwater diatoms) in response to nutrients, solar radiation and water temperature variations. It was shown that the proposed methodology is an effective one to successfully capture the reported differences among the basins of Rapel reservoir. This methodology can be further applied to study a more complete set of ecosystemic compounds present in this reservoir.

Acknowledgements

The authors wish to thank the financial support of MECESUP under project UCH0310, FONDECYT through projects 1040494 and 1080617, and the Department of Civil Engineering of the University of Chile. They also thank Profs. Irma Vila and Manuel Contreras, of the Department of Ecology of the University of Chile and the Centre for Applied Ecology, respectively, for generously providing the field data and other information used in this study, and ENDESA and DGA, Chilean Ministry of Public Works, for providing access to their hydrological and meteorological databases. Finally, we wish to thank Prof. Aldo Tamburrino and Dr. Ginger Martinez for their useful comments on an earlier draft.

REFERENCES

Ahumada, C., 2000. Diagnostic of water quality in Rapel reservoir and proposal for vigilance and monitoring. Undergraduate Thesis. Department of Civil Engineering, University of Chile (In Spanish).

Antenucci, J., 1996. Hydrobiological modelling of Rapel reservoir, Central Chile. Honours Thesis. Department of Environmental Engineering, University of Western Australia.

Artioli, Y., Bendoricchio, G., Palmeri, L., 2005. Defining and modelling the coastal zone affected by the Po River (Italy). Ecol. Model. 184, 55–68.

Bendoricchio, G., Palmeri, L., 2005. Quo vadis ecosystem? Ecol. Model. 184, 5–17.

Botelho, D., Imberger, J., 2007. Dissolved oxygen response to wind-inflow interactions in a stratified reservoir. Limnol. Oceanogr. 52, 2027–2052.

Bruce, L., Hamilton, D., Imberger, J., Gal, G., Gophen, M., Zohary, T., Hambright, K.D., 2006. A numerical simulation of the role of zooplankton in C, N and P cycling in Lake Kinneret, Israel. Ecol. Model. 193, 412–436.

CWR Centre for Water Research, 2004. Science Manual of DYRESM and DYRESM-CAEDYM. Web page: www.cwr.uwa.edu.au.

Carlson, R.E., 1977. A trophic state index for lakes. Limnol. Oceanogr. 22, 361–369.

Castendyk, D., Webster-Brown, J., 2007. Sensitivity analyses in pit lake prediction, Martha Mine, Nez Zeland 1: relationship between turnover and input water density. Chem. Geol. 244, 42–55.

Contreras, M., Villagran, H., Salazar, C., 1994. Hydrodynamic characteristics of Rapel reservoir. Medio Ambiente 12, 41–49, In Spanish.

Fischer, H., List, E., Koh, R., Imberger, J., Brooks, N., 1979. Mixing In Inland and Coastal Waters. Academic Press.

Gal, G., Imberger, J., Zohari, T., Antenucci, J., Rosenberg, T., 2003. Simulating the thermal dynamics of Lake Kinneret. Ecol. Model. 162, 69–86.

Hamilton, D., Schladow, G., 1997. Prediction of water quality in lake and reservoir. Part I—model description. Ecol. Model. 96, 91–110.

Han, B., Armengol, J., García, J., Camerma, M., Roura, M., Dolz, J., Straskraba, M., 2000. The thermal structure of Sau Reservoir (NE: Spain): a simulation approach. Ecol. Model. 125, 109–122.

Hodges, B., Imberger, J., Saggio, A., Winters, K.B., 2000. Modeling basin-scale waves in stratified lakes. Limnol. Oceanogr. 45, 1603–1620.

Imberger, J., Patterson, J., 1981. A dynamical reservoir simulation model: DYRESM 5. In: Transport Model For Inland and Coastal Waters, pp. 310–361.

Imberger, J., 2005. Practitioners Guide to Lake Management. XXXI IAHR Congress, Seoul, Korea.

Jähne, B., Haußecker, H., 1998. Air-Water gas exchange. Annu. Rev. Fluid Mech. 30, 443–468.

Jørgensen, S.E., Bendoricchio, G., 2001. Fundamentals of Ecological Modelling, third ed. Elsevier Science Ltd.

Kjaran, S.P., Holm, S.L., Myer, E.M., 2004. Lake circulation and sediment transport in Lake Myvatn. Aquat. Ecosys. 38, 145–162.

Knightes, C., Cyterski, M., 2005. Evaluating predictive errors of a complex environmental model using a general linear model and least square means. Ecol. Model. 186, 366–374.

Loose, B., Niño, Y., Escauriaza, C., 2005. Finite volume of variable shallow-water flow equations for well-mixed estuary:

application to the Río Maipo estuary in central Chile. J. Hydraulic Res. 43, 339–350.
Martinez, G., Contreras, M., Vila, I., 2003. Conceptual models for phytoplankton abundance associated with spatial heterogeneity in Rapel reservoir (Central Chile). Revista Chilena de Historia Natural 76, 255–266 (In Spanish).
Patterson, J.C., Hamblin, P.F., Imberger, J., 1984. Classification and Dynamic Simulation of the Vertical Density Structure of Lakes. Limnol. Oceanogr. 29, 845–861.
Porcasi, X., Calderón, G., Lamfri, M., Gardenal, N., Polop, J., Sabattino, M., Scavuzzo, C.M., 2005. The use of satellite data in modeling population dynamics and prevalence of infection on the rodent reservoir of Junin virus. Ecol. Model. 185, 437–449.
Robson, B.J., Hamilton, D., 2004. Three-dimensional modelling of a *Microcystis* bloom event in Swan River estuary, Western Australia. Ecol. Model. 174, 203–222.
Romero, J.R., Antenucci, J., Imberger, J., 2004. One- and three-dimensional biogeochemical simulations of two differing reservoirs. Ecol. Model. 174, 143–160.
Spillman, C.M., Imberger, J., Hamilton, D., Hyipsey, M., Romer, J., 2007. Modelling the effects of Po River discharge, internal nutrient cycling and hydrodynamics on biogeochemistry of the Northern Adriatic Sea. J. Mar. Syst. 68, 167–200.
Staskraba, M., Hocking, G., 2002. The effect of theoretical retention time on hydrodynamics of deep river valley reservoirs. Int. Rev. Hydrobiol. 87, 61–83.
Vila, I., Contreras, M., Montecinos, V., Pizarro, J., Adams, D., 1997. Rapel, 30 years temperate reservoir. Eutrophication or Contamination? Arch. Hydrobiol. Spec. Issues Advanc. Limnol. 55, 31–44.